





## Article

# Hydrological, geochemical and microbiological controls on iron mineralisation in an intermittent stream

Zackry Stevenson , Mia Riddley , Tamara McConnell and Elizabeth D. Swanner 

Iowa State University, Department of the Earth, Atmosphere, and Climate, Ames, IA, USA

## Abstract

In Clear Creek, which runs through the Iowa State University campus in Ames, Iowa, USA, several types of iron mineralisation occur within stagnant pools and slow-moving water. This includes rusty flocs, commonly observed in mineral springs, rust-stained sediments and iridescent films ('schwimmeisen') on the pool surfaces. Observations of iron mineralisation over the course of more than a year in a single reach indicated that mineralisation occurred after precipitation events once water levels in the stream had dropped. Iron extracted and quantified from Clear Creek sediments and pool waters indicated the stream and its sediments were unlikely to be supplying the iron for mineralisation. We hypothesise that the observed mineralisation could result from the discharge of shallow, reducing groundwater-bearing Fe(II) into stagnant pools that form in debris-dammed areas of the stream. Piezometers installed next to the creek documented that shallow groundwater contained dissolved Fe, with the source of Fe being the floodplain sediments and the hydraulic gradient promoted groundwater discharge into the stream. Microorganisms identified in mineralised pools using 16S rRNA amplicon sequencing revealed an elevated presence of putative iron-oxidizing and iron-reducing microorganisms in mineralised vs. non-mineralised pools. Further investigation of the iridescent films revealed them to be composed of amorphous Fe(III) minerals. We further hypothesise that microbial exudates reduce surface tension and potential micro-zones for subsequent microbial iron redox cycling with dissolved organic matter in the pools. Determining the processes controlling mineralisation can lead to a better understanding of the ecological role of iron mineralisation in agricultural watersheds and the importance of contaminant degradation and nutrient cycling.

**Keywords:** iron films; agricultural stream; iron (oxyhydr)oxide; iron-oxidizing bacteria

(Received 08 August 2024; revised 22 November 2024; manuscript accepted: 21 December 2024)

## Introduction

Streams are important conduits of elements between watersheds, downstream rivers or estuaries. A stream's chemical inputs reflect the local watershed characteristics. Specifically, the hyporheic zone is influenced by groundwater quality and neighbouring ecosystems that have an impact on the cycling of nitrogen, phosphorus and sulfur (Lawrence et al., 2013). Agricultural watersheds with forested riparian zones can enhance nitrogen and phosphorus cycling through biotic uptake, sediment deposition, agricultural runoff and seasonal dynamics (Kreiling et al., 2021). However, there is less work to address the hydrology and biogeochemistry of iron cycling in lower-order agricultural streams. Slow-moving water contributes to intermittent suspended organic material deposition, which aids in the development and maintenance of oxygen gradients in water and sediment porewaters, which can alter the mobility of iron and other redox-active trace metals (Rosenberg and Schroth, 2017). In particular, the hyporheic zone in these streams is an

interface between the anoxic and/or trace-metal-rich groundwater, with an oxidative and reductive capacity that can affect elemental cycling (Boano et al., 2014; Hoagland et al., 2020; Yang et al., 2018), including iron redox cycling (Boulton et al., 1998). Determining where and how iron enters such streams is important to identify hot spots of microbial iron and nutrient cycling, which can drive contaminant degradation or immobilisation through processes such as adsorption onto iron minerals. This is particularly important for agricultural watersheds or those with other disturbances that affect water quality and ecology.

Iron is present in Earth's surface environment as a major crustal cation, as oxides during weathering, as an ion dissolved in water, and within biological organisms as a requisite trace nutrient. Iron moves between these different reservoirs when it is transformed between its primary oxidation states (*i.e.* Fe(II) and Fe(III)) and distinct chemical species, which control the solubility and mobility of iron (Kappler et al., 2021). Seeps and springs where anoxic groundwater discharges to the oxygenated surface are hot spots for microbial redox cycling and iron mineralisation at such sites have previously been observed (Kozubal et al., 2008; Mori et al., 2015; Pierson and Parenteau, 2000). Several possibilities for iron inputs exist for creek beds and streams, including iron mobilisation within the riparian zone, from the hyporheic zone, during shallow

**Corresponding author:** Elizabeth D. Swanner; Email: [eswanner@iastate.edu](mailto:eswanner@iastate.edu)

**Cite this article:** Stevenson Z., Riddley M., McConnell T., & Swanner E.D. (2025). Hydrological, geochemical and microbiological controls on iron mineralisation in an intermittent stream. *Geo-Bio Interfaces* 2, e1, 1–16. <https://doi.org/10.1180/gbi.2025.1>

or deep groundwater discharge or inputs from the larger watershed during rain events (Lautz and Fanelli, 2008; Rivett et al., 2011; Sarkkola et al., 2013). Two other common iron sources are from acid rock drainage, where iron sulfides are weathered (Ahn et al., 2015; Dold et al., 2013), or through acid mine drainage in mine-impacted areas (Méndez-García et al., 2015).

Seeps and springs can introduce Fe(II) from anoxic groundwater, utilised by iron-oxidizing bacteria as it discharges into oxygenated water. Iron-oxidizing bacteria (FeOB) can oxidise Fe(II) to Fe(III) under both oxic and anoxic aquatic conditions and have previously been recognised as contributing to in-creek iron deposits (Emerson, 2012; Roden et al., 2012). Freshwater environments with circumneutral pH are generally dominated by FeOB within the *Gallionellaceae* family (e.g., *Gallionella capsiferiformans*) (Almaraz et al., 2017; Roden et al., 2012). By contrast, *Sideroxydans* sp. are FeOB found in acidic and circumneutral environments (Fabisch et al., 2013; Roden et al., 2012). Moreover, these FeOB make up flocculent iron mats in various freshwater systems (Brooks and Field, 2020). In circumneutral pH and oxygenated conditions, Fe(III) is the favoured valence, which is relatively insoluble and forms Fe(III) (oxyhydr)oxides (Cornell and Schwertmann, 2003; Sobolev and Roden, 2002). *Acidithiobacillus* and *Lepstospirillum* have been found in acidic streams and are known FeOB that contribute heavily to iron oxidation in these systems (Méndez-García et al., 2015). Variations in pH, nutrients, oxygen content and organic matter inputs can control the identity and compositions of Fe(III) (oxyhydr)oxide minerals, which then provide electron sources for various iron-respiring organisms (Bruun et al., 2010; Chan et al., 2016; Emerson et al., 2010; Roden et al., 2012). Oxygen-poor conditions could result from water stagnation and particulate organic carbon input, allowing iron-reducing bacteria (FeRB) to reductively dissolve mineralised Fe(III) (Brooks and Field, 2020; Dubinsky et al., 2010; Lovley, 1987). Floating surface films of iron have been detected in multiple seeps, springs and creeks and could be a hotspot for microbial activity (Almaraz et al., 2017; Dong et al., 2024; Grathoff et al., 2007; Sánchez-España et al., 2023). However, the oxidation state and mineralogy of floating iron films are not well-characterised, and there is conflicting evidence on whether these formations are Fe(II), Fe(III) or a mixture of both (Dong et al., 2024; Grathoff et al., 2007; Perkins et al., 2016). Furthermore, there is little comparative work on the microbial community composition associated with floating iron films vs. flocculent iron mats or other types of in-creek iron mineralisation.

This study reports observations of iron mineralisation in an intermittent stream located in Ames, Iowa, USA to provide a combined hydrological, geochemical and microbiological investigation of iron sources and microbial redox cycling. This stream is of particular interest because it is in an agricultural watershed, and iron-cycling organisms can play a role in organic pollutant (e.g. herbicide) degradation or nutrient cycling. Our goals were to (1) inform the source of iron to the stream, (2) document the geochemical conditions that give rise to the observed iron deposits, (3) investigate the microorganisms associated with the iron mineralisation types and (4) resolve the oxidation state and mineralogy of iron in floating iron films. These results will elucidate the impact of hydrology, geochemistry and microbiology on in-stream iron cycling and mineralisation.

## Methods

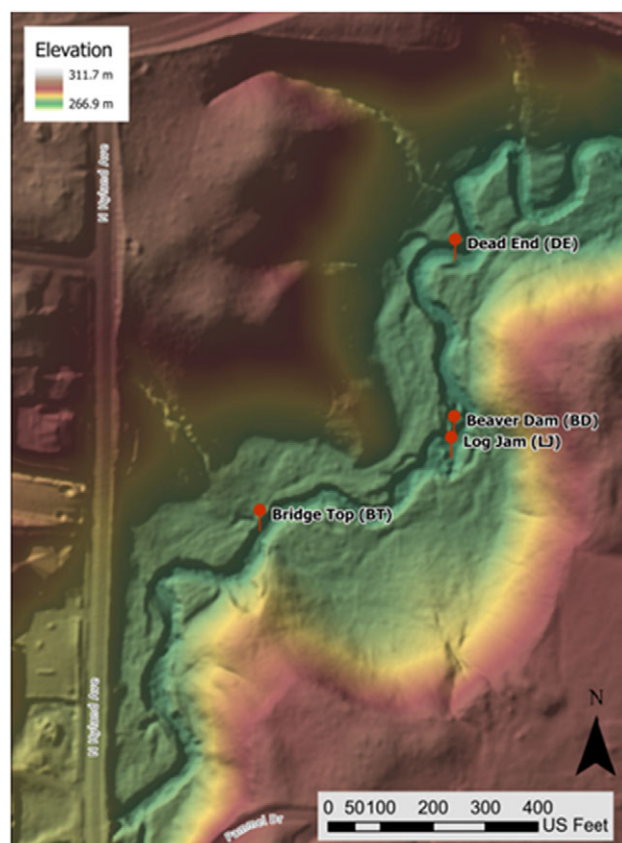
### Field description

Clear Creek is a small Iowa Creek tributary in Ames, Iowa and part of the Des Moines lobe of the Wisconsin-aged glaciation. Clear Creek has intermittent iron mineralisation forming

predominantly within stagnant pools. Four areas with intermittent but recurring iron mineralisation were identified within a 0.20-mile reach of the stream running through the Iowa State University campus. The upstream site is Bridge Top (BT) (42° 01' 54.90012" N 093° 39' 16.30008" W), the two midstream sites are Log Jam (LJ) (42° 01' 56.306658" N 093° 39' 11.470572" W) and Beaver Dam (BD) (42° 01' 56.70012" N 093° 39' 11.40012" W) and the downstream site is Dead End (DE) (42° 01' 58.583388" N 093° 39' 11.4695028" W) (Figure 1). Each site had different iron accumulation patterns that may have been related to in-stream debris and water flow paths. Over the past decade, the creek has experienced a maximum 24-hour precipitation of 11.38 cm, with a mean annual precipitation of 87.35 cm (USGS, 2022).

### Piezometers

Two piezometers were installed in April 2024 to characterise the soils near the stream and determine the iron concentrations in groundwater and soil. The first piezometer was installed near the stream at coordinates N 42.03220 and W 093.65303. The second one is within 5 m of the first one, but further from the creek at coordinates N 42.03228 and W 093.65314 (Supplemental Figure 1). A bucket auger was used to remove subsequent ~20 cm soil cores until hitting the water table. Soil cores were aligned sequentially and characterised using the Munsell colour chart. Soil samples were collected from alternating sections from the surface to the water table, placed in whirlpack bags and frozen at -20°C until further analysis for iron concentrations.



**Figure 1.** LiDAR map of Clear Creek on Iowa State University's campus in Ames, Iowa, USA, produced in ArcGIS. Plotted locations are sample sites. Stream flows to the northeast.

### Observations and geochemical measurements

Observations of iron mineralisation and geochemical measurement sampling were done in tandem at each site at least weekly when temperatures were above freezing during the study period (October 2021 to December 2023). When frozen, the creek was observed and/or sampled at monthly intervals. During the open water season, observations were made no more often than every three days with at least a three-day gap between observations.


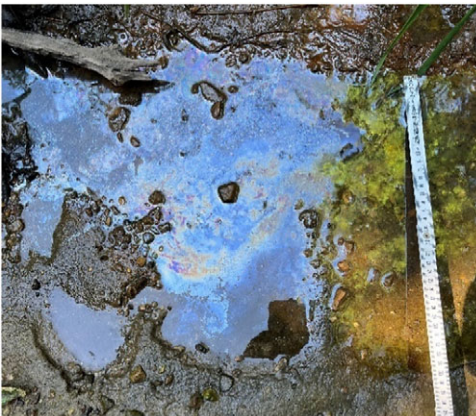

Physicochemical measurements of pools were made using a YSI ProDSS multiparameter probe. The measurements included dissolved oxygen (DO;  $\text{mg L}^{-1}$ ), temperature ( $^{\circ}\text{C}$ ), specific conductance ( $\mu\text{S cm}^{-1}$ ), pH, and Oxidation-Reduction Potential (ORP). For piezometer data collection, the YSI ProDSS was lowered to the

water table for data collection. Clear Creek was sampled at the same time as the piezometers. When there was visible iron in the sampling pools, the observed iron type (Table 1) was recorded and the pool volume was estimated based on the dimensions of the two longest axes of each pool and its maximum depth.

### Phosphorous quantification

Total phosphorus (TP) and orthophosphate (OP) were determined in both water table samples from the piezometers and from Clear Creek using a modified TP and OP method from Murphy and Riley (1962). For piezometers, a bailer was used to fill 15 mL conical tubes, and separate 15 mL conical tubes were dipped into pools in Clear Creek. Samples were brought back to the lab and analysed

**Table 1.** Iron mineralisation types. Scale bars are in centimetres.

Mineralisation Type	Description	Image of iron mineralisation type
Flocculent iron mats	Soft, fluffy orange-brown mat attached to sediment surfaces that has the appearance of wet peanut butter. Found in areas of low or no flow.	
Iridescent films ('schwimmeisen')	Floating iridescent and/or metallic surface films that resemble oil but break up upon disturbance, unlike oil. Found only in stagnant pools.	
Solid mineral precipitates	Bright orange minerals staining the sediment surface of stagnant pools.	

right away. For OP, water was filtered with a 0.45 µm filter into a new 15 mL conical tube. To determine OP, a fresh phosphorus colour reagent was made by adding sulfuric acid solution, potassium antimony tartrate solution, ascorbic acid solution and molybdate solution. After 30 minutes of dark incubation, samples were analysed on an Epoch 2 Microplate Reader (Biotek) at 885 nm. TP was determined with a 1.6% solution of potassium persulfate. Tubes were placed in the autoclave for 30 minutes at 121.5°C. Tubes were cooled to room temperature before following the same procedure as OP for analysis of TP at 885 nm.

### Iron quantification

Two methods were used to quantify total iron in the water. Unfiltered samples were collected in a 15 mL conical tube. Samples taken immediately back to the lab were prepared for quantification using the Hach TNT 890 Metals Prep Set. Iron concentrations were determined using the TNT 858 method on a Hach DR1900 Portable Spectrophotometer. For the second method, unfiltered water was collected in a 15 mL conical tube and immediately acidified with 6M hydrochloric acid (HCl) to a final concentration of 1M HCl. Ferrous iron [Fe(II)] was determined with the Ferrozine assay following a protocol adapted from Stookey (1970) and Viollier *et al.*, (2000) using an Epoch 2 Microplate Reader (Biotek). Total ferrous iron [Fe(II)] was determined with the Ferrozine assay, and then again after hydroxylamine hydrochloride reduction to determine total Fe. Then, Fe(II) was subtracted from total Fe to determine Fe(III). Samples were diluted if concentrations exceeded the detection range (10–300 µM).

Pool sediments were sampled into 15 mL conical tubes for iron extractions. If not processed immediately, samples were stored in a –80°C freezer. Thawed or newly collected samples were placed in a Captair Pyramid 2200A Multi-function Disposable Glovebox flushed with N<sub>2</sub> gas (Erlab, #17404CN) for Fe extraction to prevent speciation changes in iron due to the presence of oxygen. In the glove bag, half a gram of wet sediment was weighed and placed into stoppered serum bottles. Anoxic sodium acetate solution (25 mL) was added to the bottles and shaken at room temperature for 1 hour to solubilise the sorbed iron from sediments. After centrifugation for 20 minutes at 2300 g, the supernatant was extracted to quantify sorbed iron with Ferrozine as described above. The crystalline ferrous phase was extracted with 25 mL of anoxic 6M HCl. For this treatment, samples were shaken for 24 hours at room temperature and centrifuged to extract the supernatant. Both extractions were analysed with the ferrozine assay to quantify iron. Three sub-samples were extracted from each sample for triplicate measurements.

Soils that were frozen after piezometer installation were processed similarly to the pool sediments, with one change to the protocol. One gram of soil was weighed and placed into a serum bottle instead of 0.5 g for better detection of the low-quantity adsorbed fraction.

### Microbial community analysis

To investigate the microbial community of pools, 500 mL of water was passed through a series of sequential filters (11 µm nylon and 3 and 0.22 µm PES filters; Millipore) with a Masterflex Portable Peristaltic Sampler (Cole/Parmer). The 11 µm filter captured larger phytoplankton, and this study did not investigate these samples further. The 3 and 0.22 µm were expected to capture particle-associated and planktonic microbial cells, respectively.

Filters were stored at –80°C in cryovial tubes with RNAlater™ (Lambrecht *et al.*, 2020). Total community DNA was then extracted from the biomass on the filters using a modified DNeasy Powerbiofilm Kit: the original centrifugation step was omitted as the entire filter was used. Also, 30 µL of elution buffer was used instead of the recommended 100 µL to concentrate the DNA. Prior to sample submission, DNA concentration was quantified by a Qubit 2.0 Fluorometer at the Iowa State University DNA sequencing facility. All samples were diluted to a concentration of ~20 ng. The V4 region of the 16S rRNA gene was amplified using the primer pair 515 F (5'-GTGCCAGCMGCCGCGGTTAA-3') and 805R (5'-GACTACVSGGGTATCTAAT-3') using a dual index approach (Kozich *et al.*, 2013). Samples were sequenced on an (Illumina Miseq) using 2 × 250 bp at the Iowa State University DNA Facility.

Sequences were trimmed and quality screened using the DADA2 package in R (Callahan *et al.*, 2016). Forward and reverse sequences were trimmed at 225 and 195 bases to account for differences in quality plots of reverse and forward reads. Reads were denoised, merged and screened for chimeric sequences for removal and Amplicon Sequence Variants (ASVs). The *phyloseq* package was used to create the taxonomy and sample table for further analysis (McMurdie *et al.*, 2013). The *decontam* package was used to identify and remove ASV associated with negative controls (Davis *et al.*, 2018). Negative controls from an elution buffer and water were run through the same DNA isolation kit and evaluated using the prevalence method. A threshold value of 0.5 was set and used to create a new *phyloseq* object. We assigned taxonomy with an updated cyanobacteria inventory, *Cyanoseq* database, which encompasses the *Silva* database (CyanoSeq 1.2; Silva 138.1) for better accuracy of this phylum (Lefler *et al.*, 2023). For further analysis, sequencing reads from the 0.22 and 3 µm filters were pooled for each sample. The relative abundance of microbes was rarefied and all organisms were grouped into an 'other' category, while putative iron-reducing and oxidizing ASVs were graphed separately to interpret abundance change in samples. Principal Coordinates Analysis (PCoA) was conducted in *phyloseq* using the default Bray-Curtis dissimilarity, and differences were declared significant based on p-values <0.05. All sequences from the tagged Illumina MiSeq libraries were submitted to the NCBI short-read archive under the bioproject number (PRJNA1053376).

### Scanning Electron Microscopy and Transmission Electron Microscopy analysis

Field-Emission Scanning Electron Microscopy (FE-SEM) was used to image iridescent films. The iridescent film was scooped onto a silica oxide wafer. Samples were analysed both without preventing oxygen and exposure and by keeping anoxic. In the second case, the sample was transported in a Pyrex container with an AnaeroPack (Fischer Scientific) prior to placing it in an anoxic glovebox (100% N<sub>2</sub>) to prevent further oxidation before analysis. Images of the iridescent iron film deposited on the wafer were analysed using a ThermoFisher (FEI) Teneo Lovac microscope at the Ames National Laboratory's Sensitive Instrument Facility. Secondary electron images were taken of the stub on low magnification with no coating and low vacuum mode. Back-scatter images were taken at varying accelerating voltages of 1, 3, 15 and 20 kV, and a high magnification low voltage was used to image the film 'crust'. Additional images were taken in Optiplan mode and high vacuum/standard mode using a Lo-vac Detector (LVD) or an Everhard-Thornley Detector (ETD).

For transmission electron microscopy (TEM) analysis, an acid-washed petri dish was used to scoop water with an iridescent film and then placed in a glass Pyrex container with an Anaero-Pack (Fischer Scientific), which reacted with any trace oxygen in the container to maintain an anoxic atmosphere during transport so no further oxidation occurred before analysis. The FEI Titan Themis Cubed Aberration Corrected Scanning Transmission Electron Microscope (STEM) was utilised to acquire TEM images of the films. The sample was placed on a copper grid with a carbon film. Energy dispersive spectroscopy (EDS) was used to determine the elemental composition of the films. The FEI Tecnai G2-F20 scanning transmission electron microscope was utilised for Selected Area Diffraction Patterns (SADP) to obtain diffraction patterns of iridescent films to determine the mineralogy based on available reference data. High-angle Annular Dark Field (HAADF) was paired with Electron energy loss spectroscopy (EELS) to obtain high-contrast images and determine iridescent films iron oxidation state and chemical composition. Reference spectra for the iron oxidation state were made with 2-line ferrihydrite [Fe(III)] (precipitated according to Schwertmann and Cornell, 1991) and hercynite (predominantly Fe(II), but our sample probably contained some Fe(III)).

## Results and discussion

### Iron mineralisation

Observations across a year-long sampling period led to the categorisation of three main iron mineralisation types within four sites of Clear Creek (Table 1).

Flocculent iron mats were found in the midstream sites (LJ and BD). Multiple studies have found flocculent mats in different aquatic habitats ranging from neutral groundwater seeps, sea mounts, deep hydrothermal vents or roadside ditches (Emerson and Revsbech, 1994; Rentz et al., 2007; Roden et al., 2012). Flocculent iron mats that house FeOB play a significant role in the biogeochemistry of the environments in which they occur through the degradation of organic compounds and pesticides and the removal of heavy metals and phosphorous (Fabisch et al., 2013; Rentz et al., 2009).

An iridescent surface film was found only at stagnant pools in the midstream sites. In the literature, these films have been called 'schwimmeisen', German for 'floating iron' (Grathoff et al., 2007). However, multiple studies have also observed an iron 'sheen'

that sits on top of stagnant water (Almaraz et al., 2017; Perkins et al., 2016; Sánchez-España et al., 2023). Moreover, it has been observed that rainfall and wind will disturb these films (Grathoff et al., 2007).

Lastly, rust-coloured solid mineral precipitates were found in some sample sites.

### Temporal in-stream hydrological and geochemical conditions

Clear Creek was repeatedly sampled at four unique locations for water chemistry, iron concentrations and speciation in water and sediments, and observations of the three iron mineralisation types throughout a single year across three seasons. Locations of sampling sites are found in Figure 1, while the pool characterisation data is found in Table 2.

Site BT (Figure 1), furthest upstream, was near the start of the deciduous forest zone of our sampling area. The site had small accumulations of organic debris near the stream's edge where the water was not obstructed. Consistent flows were observed throughout sampling, although only a small pool remained during prolonged dry periods. Dissolved Oxygen (DO) was consistently above 7 mg L<sup>-1</sup>, but this site had the lowest specific conductivity of all sites throughout the sampling period, ~400 µS cm<sup>-1</sup> (Figure 2).

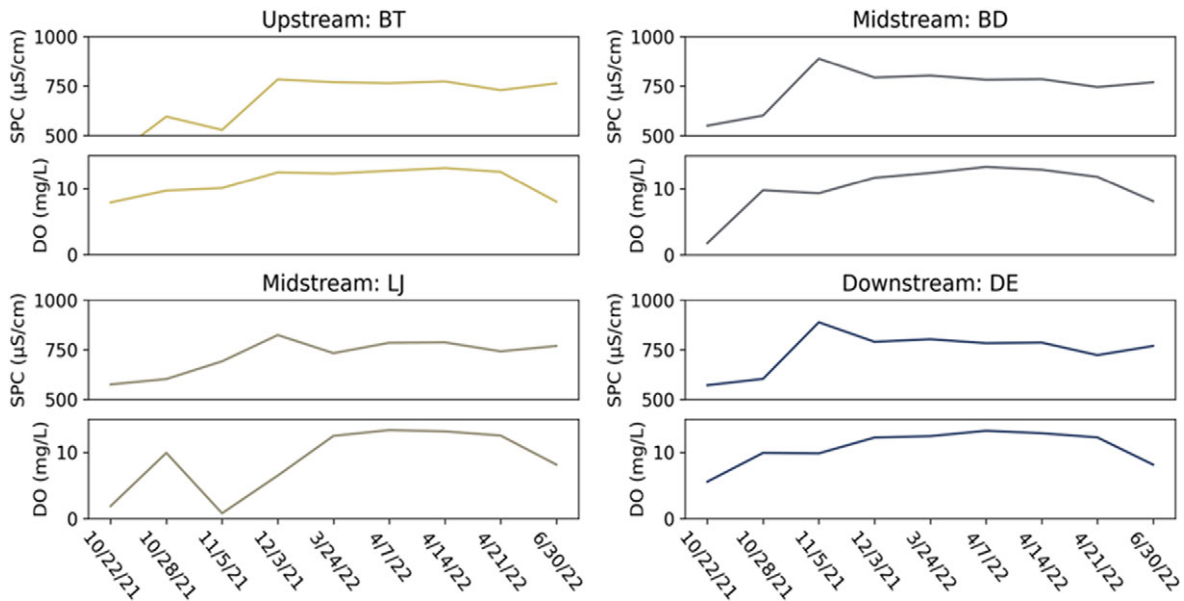
The midstream sites LJ and BD (Figure 1) were impacted by wood and organic debris that created small dams, effectively slowing the water flow through these two stretches and creating pools. The midstream sites had the lowest DO concentrations during October 2021, <2 mg L<sup>-1</sup> (hypoxic). Specific conductance was also consistently >500 µS cm<sup>-1</sup> at these sites during all sampling periods (Figure 2). Increased specific conductance from the upstream site (BT) to the midstream sites (LJ and BD) indicates the input of an additional water source with higher dissolved solutes. There are no surface inlets along any of the four sites (Figure 1).

Downstream site DE (Figure 1) had similar specific conductivity measurements as the midstream sites >500 µS cm<sup>-1</sup> (Figure 2). However, the DO concentrations were consistently above ~4 mg L<sup>-1</sup> (Figure 2). Like the upstream site, little debris obstructed the water flow. The higher specific conductance at site DE compared to the upstream site BT was probably due to sourcing water from the pools developed in sites LJ and BD.

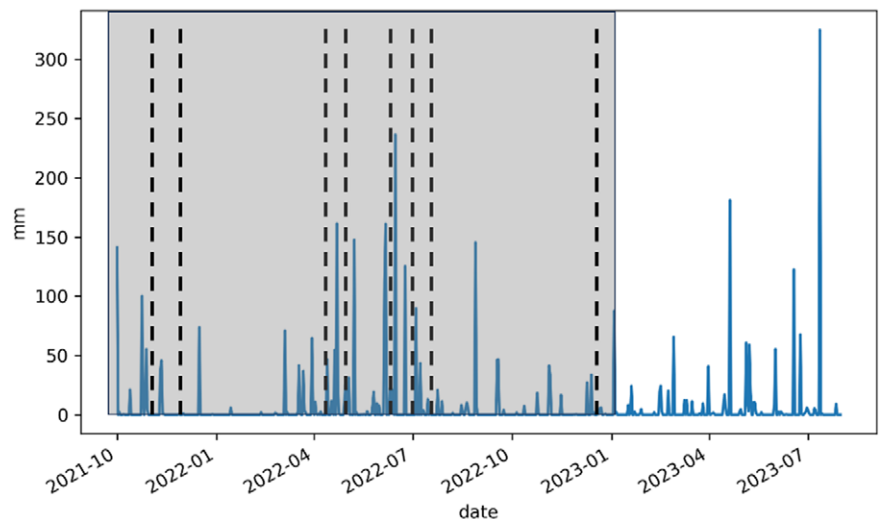
Precipitation data were retrieved from the Ames Municipal Airport (KAMW) in Ames, Iowa, and the Automated Surface Observing System (ASOS) data was downloaded from Iowa

**Table 2.** Persistent pool locations and features. Characterisations of iron persistence will be identified based on Table 1. Includes size of the pool, stagnant or flowing water, or iron types. Areal extent of iron was based on average measurements of the pool area with measuring tapes as seen in Table 1.

Pool Name	Location	Water Flow	Iron Types	Areal extent of visible iron
Bridge Top (BT) Upstream	42° 01' 54.90012" N 093° 39' 16.30008" W	Medium flow into a stagnant side pool	Little mineralisation	Small area 65–130 cm <sup>2</sup>
Log Jam (LJ) Midstream	42° 01' 56.306658" N 093° 39' 11.470572" W	Stagnant to low flow during rain events, stagnant pools after rain	Iridescent films and precipitates	Large area 150–230 cm <sup>2</sup>
Beaver Dam (BD) Midstream	42° 01' 56.70012" N 093° 39' 11.40012" W	Low flow on the dammed side; medium flow on the upstream side	Iridescent, flocculent and precipitates (medium flow)	Large area 230–310 cm <sup>2</sup>
Dead End (DE) Downstream	42° 01' 58.583388" N 093° 39' 11.4695028" W	High flow with a meander	Little mineralisation (only 2 days of visible iron)	N/A



**Figure 2.** Each site listed in Table 2 was measured once at each sampling time for specific conductivity (SPC) and dissolved oxygen (DO).

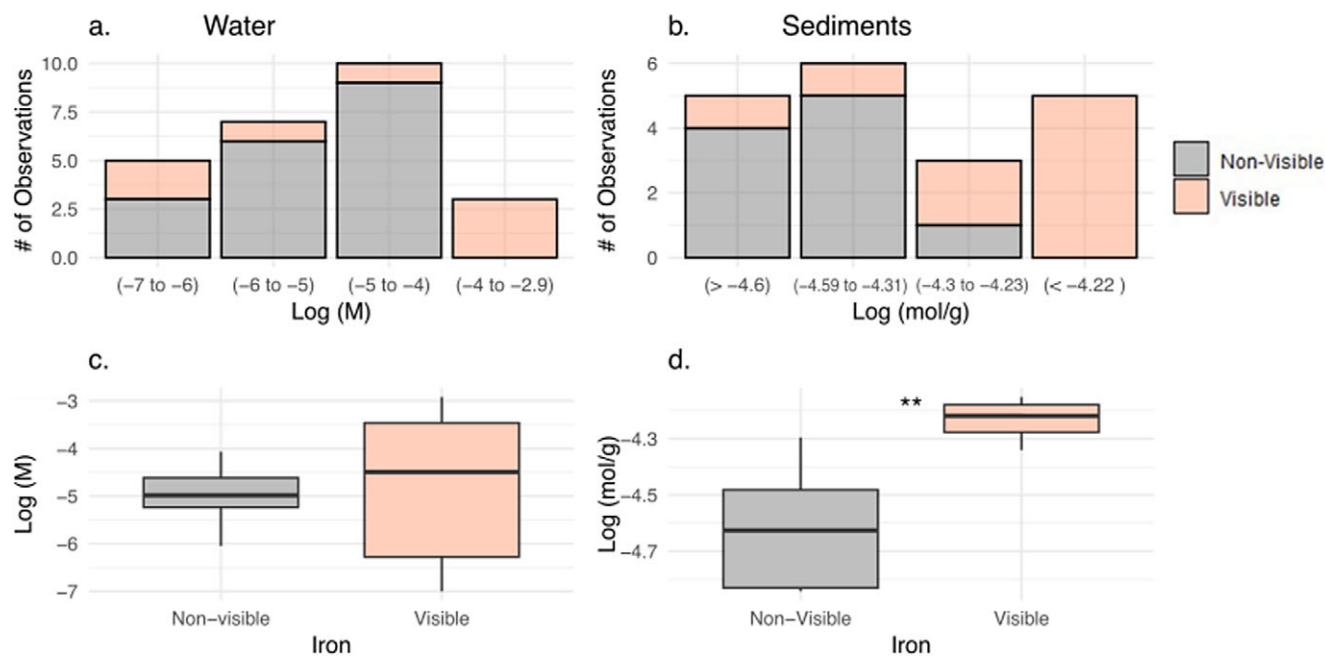


**Figure 3.** Average precipitation based on weather data collected from the local system. The dashed lines indicate times when iron mineralisation types were visible. A grey box indicates the time frame for observations of iron mineralization with geochemical data presented in Figures 2 and 5.

State University's Mesonet (<https://mesonet.agron.iastate.edu/request/download.phtml>). Publicly available rainfall records over three seasons, from October 2021 to July 2023, are presented in Figure 3. Regular monitoring observations during the open water season indicate that iron mineralisation occurred in the stream days after rain events, but not when the creek was dry. At the end of 2021, several precipitation events were followed by visible mineralisation (dashed lines in Figure 3). Little precipitation fell from January until March 2022, and the stream was frozen. Precipitation and snowmelt enhanced observed creek flows and iron mineralisation was observed in the weeks after. Very little rain fell from late May to early June 2022, leading to a dry creek bed and no iron mineralisation. Mineralisation was observed again after several multi-inch rainfall events in December 2022. However, mineralisation was not observed following a 9-inch rainfall event in late June 2022. This is probably due to high flows preventing standing pools of water, as mineralisation was typically observed in standing pools and/or high flows washing away mineralisation.

#### *Processes for enhancing iron concentrations in mineralised pools*

We wanted to understand if iron in the pools was mobilised from rain and direct runoff or added from sediments or groundwater. Enhanced iron contents and mineralization in the creek could result from runoff transporting iron from the watershed into the creek and pools. Previous work on the Corbeira catchment in NW Spain found that higher rainfall years led to increased Fe loads in the stream compared to lower rainfall events coinciding with lower Fe loads (Soto-Varela *et al.*, 2015). Increased precipitation can correlate with elevated dissolved iron levels, along with varied colloidal iron, compared to dry events (Rosenberg and Schroth, 2017; Zhang *et al.*, 2020). If this were the case, we would predict similar total iron concentrations in water from the pools with and without visible iron mineralisation (Figure 4). There was no statistical difference in total iron concentrations from water in pools with visible iron mineralisation than those without (Figure 4), indicating that the water in the pool is unlikely to supply iron for mineralisation.



**Figure 4.** Histogram comparing visible and non-visible mineralisation of iron frequency and range of total iron concentrations in (a) water or (b) sediments. Box and whisker plot depicting ranges of iron concentrations in (c) water or (d) sediments. Stars indicate statistically significant values (\*\* $p < 0.01$ ).

Consistently oxic conditions in the upstream and downstream sites with flowing water indicate that any dissolved Fe(II) would be oxidised to Fe(III) and rapidly precipitated in circumneutral waters, resulting in minimal in-creek transport. Our methods did not specifically assess the presence of complexed or colloidal iron that could be transported simultaneously with the dissolved load of the creek.

However, there was a significant increase in the amount of iron within sediments of pools with visible iron mineralisation compared to those without. The higher iron content in mineralised sediments indicates that iron must be added to the mineralised pools from another source besides pool or creek water (Figure 4). A process that adds iron to the creek sediments is required to explain the observation that visibly mineralised pools have higher sedimentary iron contents but not higher water iron contents. A plausible mechanism is needed for the discharge of anoxic groundwater bearing dissolved Fe(II) from the surrounding soils/sediments and/or hyporheic circulation of creek water, picking up dissolved Fe(II), as seen from the soil and groundwater Fe concentrations (Figure 5). Groundwater inputs and/or enhanced hyporheic exchange would increase dissolved ions relative to water from precipitation and inputs could account for the higher specific conductance values (Figure 2) in the midstream sites (LJ, BD) relative to the upstream site (BT). The lowest DO values in midstream sites (LJ and BD) also correspond to times when mineralisation occurred and are consistent with either the discharge of anoxic groundwater or the development of reducing conditions that could draw down in pool DO. Notably, the mean percentage of baseflow to annual stream flow in Clear Creek is 53.98%, underscoring the substantial contribution of groundwater discharge to the water budget of the system (USGS, 2022).

Clear Creek receives water from precipitation amended with groundwater discharge and runoff from surrounding sediments and deciduous vegetation. Research in northeastern Belgium at the Kleine Nete catchment found that increased base flow

introduces enriched Fe(II) groundwater, which is oxidised and precipitated on the stream bed (Baken et al., 2015). Another site with iron mineralisation – West Berry Creek in Santa Cruz, California, USA – has an average regional precipitation of less than ~2.5 cm and also probably receives iron inputs from groundwater (Duckworth et al., 2009). The damming effect at sites LJ and BD in Clear Creek could have created a longer hydraulic residence time of stream water, enhancing hyporheic exchange or shallow groundwater recharge/discharge. Similarly, beaver dam sites in Coal Creek and East River, Colorado, USA had higher specific conductivity in groundwater compared to the stream, with recharge flows transporting dissolved Fe(II) to stream beds (Briggs et al., 2019).

Shallow groundwater could provide a source of dissolved Fe(II) due to microbial reductive dissolution of Fe(III) (oxyhydr) oxides with organic carbon within the floodplain sediments. These floodplain sediments adjacent to Clear Creek are materials such as silt and clay that can naturally accumulate leaf litter and wood debris over time. Water infiltrates the floodplain during high rainfall, and the ensuing anoxia allows microbial Fe(III) reduction with clay materials and organics due to the high surface area and saturated environment to enhance Fe(II) mobilisation (Figure 5). Rainwater mobilises this Fe(II), allowing a recharge to the groundwater due to the porosity of the deeper floodplain sediments composed of massive pebbly sand and massive gravelly sand (Figure 5). Soils surrounding Clear Creek are >98% soil Type B from the Soil Survey Geographic Database (SSURGO), composed of sandy soils, an above-average infiltration and less aggregated loess (Figure 5; USGS 2022). The rising water table establishes the hydraulic gradient, causing Fe-rich groundwater to flow into the creek.

The sediments retrieved during piezometer installation had noticeable iron mineralisation at the water table. The piezometers were placed within 5–8 m of the creek, upgradient due to high ground on an adjacent hillslope. In September 2024, the water table elevation measurements in both wells indicated shallow groundwater flow toward the stream with a hydraulic gradient

Piezometer Well #1, nearest to Clear Creek					Clear Creek Average Geochemical Conditions
Depth (m)	Soluble Fe fraction (log mol/g)	Total Fe mineral fraction (log mol/g)	Soil Type *Subangular blocky (SBK)	Munsell color scale	
0 – 0.20	-5.66	-4.17	Granular silty clay	10YR2/2	pH 8.01 ± 0.36
0.20 – 0.41			SBK silty clay	10YR2/2	ORP 181.53 ± 12.72 mV
0.41 – 0.61	-4.83	-4.09	SBK silty clay	10YR2/2	SPC 762.14 ± 38.82 μS cm <sup>-1</sup>
0.61 – 0.81			SBK silty clay	10YR2/2	DO 11.96 ± 0.87 mg L <sup>-1</sup>
0.81 – 1.02	-5.48	-3.82	SBK silty clay	10YR2/2	Temp 13.1 ± 0.83 °C
1.02 – 1.22			mottled, SBK sandy clay	10YR2/2	OP 65.05 ± 3.14 μg L <sup>-1</sup>
1.22 – 1.42	-5.12	-3.66	mottled, SBK sandy clay	10YR2/2	TP 116.51 ± 13.91 μg L <sup>-1</sup>
1.42 – 1.63			mottled, SBK sandy clay	10YR2/2	OP/TP ratio 0.61 ± 0.075
1.63 – 1.83	-5.46	-4.39	Massive loam	5Y2.5/1	
1.83 – 2.03			Massive sand	2.5Y3/2	
2.03 – 2.24	-5.84	-5.04	Massive sand	2.5Y3/2	
2.24 – 2.44			Massive pebbly sand	7.5YR3/4	
2.44 – 2.64	-5.21	-4.18	Massive pebbly sand	7.5YR3/4	
2.64 – 2.85			Massive gravelly sand	7.5YR3/2	
2.85 – 3.05	-5.31	-3.99	Massive gravelly sand	7.5YR3/2	
Water Table	OP = 20.83 ± 1.07 μg L <sup>-1</sup>	pH = 6.92 ± 0.07	SPC = 922 ± 30.74 μS cm <sup>-1</sup>	DO = 1.02 ± 0.17 mg L <sup>-1</sup>	
Total depth below surface = 3.35 m	TP = 57.27 ± 1.39 μg L <sup>-1</sup>	ORP = 181.2 ± 33.34 mV	Total Fe = 46.64 ± 12.95 μM	Temperature = 13 ± 0.17 °C	
Depth to water table = 1.42 m	OP/TP ratio = 0.36 ± 0.01				

**Figure 5.** Representative sediment characteristics ascertained during piezometer installation and the resulting groundwater geochemistry within the piezometer (blue shading). Abbreviations: Dissolved Oxygen (DO), Oxidation-Reduction Potential (ORP), Specific Conductance (SPC), Orthophosphate (OP) and Total Phosphorous (TP) are represented within the table. Averages of Clear Creek geochemical data compared to the same time point of piezometer sampling appear as a sidebar.

of 0.07245 m m<sup>-1</sup>. Our data indicates a plausible mechanism for the introduction of Fe(II) into the creek through shallow groundwater discharge that is elevated in the days following precipitation events, noticeable as iron mineralisation, but after the runoff through the creek subsided enough so mineralisation is not washed away.

Soil samples from the piezometer installation were used to determine the iron fractions in each soil type to test for Fe availability (Figure 5). Loosely adsorbed iron fractions ranged from -5.84 to -4.83 log mol/g, with the highest concentration found in the depth interval of 0.41–0.61 m below the ground surface (Figure 5). The total Fe mineral fraction exhibited higher concentrations, ranging from -5.04 to -3.66 log mol/g (Figure 5). These numbers are consistent with previous literature on sandy soils from Iowa, where free iron in whole soils was between -4.90 to -4.10 log mol/g (Folks and Riecken, 1956). Moreover, a report by (Rowden, 2010) indicated on average deep Iowa soils contained -3.32 log mol/g Fe and -3.38 log mol/g Fe in shallow soils.

The wells were screened over the entire interval to capture the water table. The water was analysed for various geochemical parameters to identify differences between the in-stream profiling. Orthophosphate (OP) averaged 20.83 μg L<sup>-1</sup>, and total phosphorus (TP) averaged 57.27 μg L<sup>-1</sup> (Figure 5). These findings align with a larger-scale study of different streams and river systems around Iowa, which report OP concentrations ranging from 40–210 μg L<sup>-1</sup> OP and TP concentrations between 280 and 550 μg L<sup>-1</sup> TP (Schilling *et al.*, 2017). Notably, Clear Creek had on average higher OP/TP ratios than groundwater, suggesting an external source of P loading to the system. This could be indicative of soil erosion, runoff or due to the watershed being predominantly agricultural (Fox *et al.*, 2016; Gentry *et al.*, 2007). However, some geochemical parameters differed between in-stream and groundwater measurements. For instance, dissolved oxygen in piezometers was consistently lower on average (1.02 ± 0.17 mg L<sup>-1</sup>) than the in-creek sampling sites (11.96 ± 0.87 mg L<sup>-1</sup>), and the pH was (6.92 ± 0.07) compared to (8.01 ± 0.36) in the creek (Figure 5). These parameters indicate a reducing environment, which could supply Fe(II) to the stream.



### Putative Fe-cycling microbial community

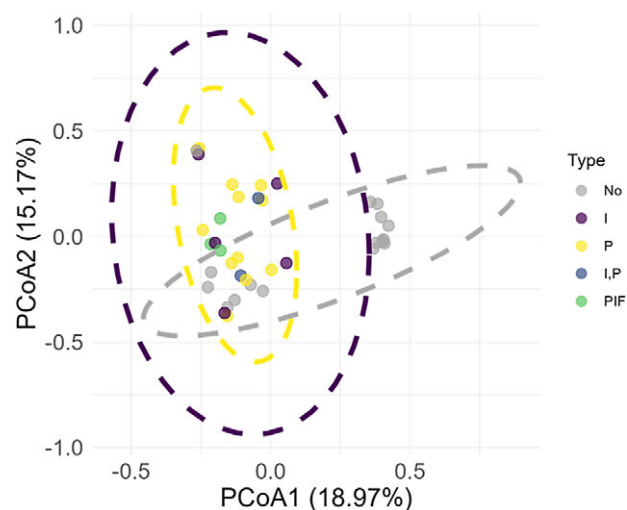
Our data support the hypothesis that recent rainfall drives enhanced groundwater discharge and/or hyporheic exchange, particularly through dammed sections of the stream, bringing in a source of dissolved Fe(II) to the pools from the surrounding soils and sediments that result in visible mineralisation. Discharge of Fe(II) can promote the development of in-pool iron mineralisation by microbes such as FeOB. Inputs of organic carbon, such as are supplied from in-creek wood, could support heterotrophic microbes and FeRB. This has been documented in streams with organic debris or beaver dams, which divert water through sediments and result in iron staining (Briggs et al., 2019; Lautz et al., 2006). Both Fe(II) and Fe(III) in Clear Creek's sediments suggest active redox cycling of iron.

We therefore assessed whether putative Fe(II) oxidizing and/or Fe(III) reducing microbes were more prevalent in mineralised vs. non-mineralised pools. Moreover, previous work on regenerative stream water conveyance structures found flocculant mat formations forming near site structures where groundwater carries Fe(II) leaching from constructed material promoting FeOB growth (Williams et al., 2016). Iron seeps located in Prince William County, Virginia, USA discharged anoxic, Fe(II) rich groundwater to the microbial community, aiding in co-occurring iron mineralisation and microbial mats (Rentz et al., 2007).

The sequencing of 16S rRNA was performed on 22 water samples from pools with visible mineralisation and 17 water samples from pools with no visible mineralisation. The samples from pools that contained visible iron mineralisation were further demarcated based on the mineralisation type present during sampling: I: iridescent (5); P: precipitates (12); I, P: both iridescence and precipitates (2); and PIF: all three iron types but dominated by flocculant iron mats (3). Further analysis determined grouping differences through microbial richness, evenness and relative abundance. Four samples were removed from further analysis due to inadequate initial library sizes <40,000 due to control samples containing an equal or greater number of sequences. A total of ~200 contaminant taxa were removed from the remaining samples after decontamination.

The Shannon, Simpson and Chao1 indexes determined the alpha diversity of visibly mineralised and non-mineralised samples (Supplemental Figure 2). Principle Coordinates Analysis (PCoA) using the Bray-Curtis dissimilarity data between iron types revealed two major clusters (Figure 6). The first (left) cluster was comprised mostly of all visibly mineralised samples, with some non-mineralised samples. A second (right) cluster contained exclusively not visibly mineralised samples (Figure 6). Based on a Permanova analysis, there was a significant difference ( $p < 0.05$ ) between the left and right clusters (Figure 6). This clustering was not related to site location (Supplemental Figure 3). However, a significant difference was observed by the season of observation ( $p < 0.05$ ; Supplemental Figure 4). Only samples collected in winter non-mineralised samples were in the right cluster, although some winter non-mineralised samples did occur in the first cluster (Supplemental Figure 4). This analysis indicates that mineralisation and season were possible drivers of microbial community composition, which is explored further below.

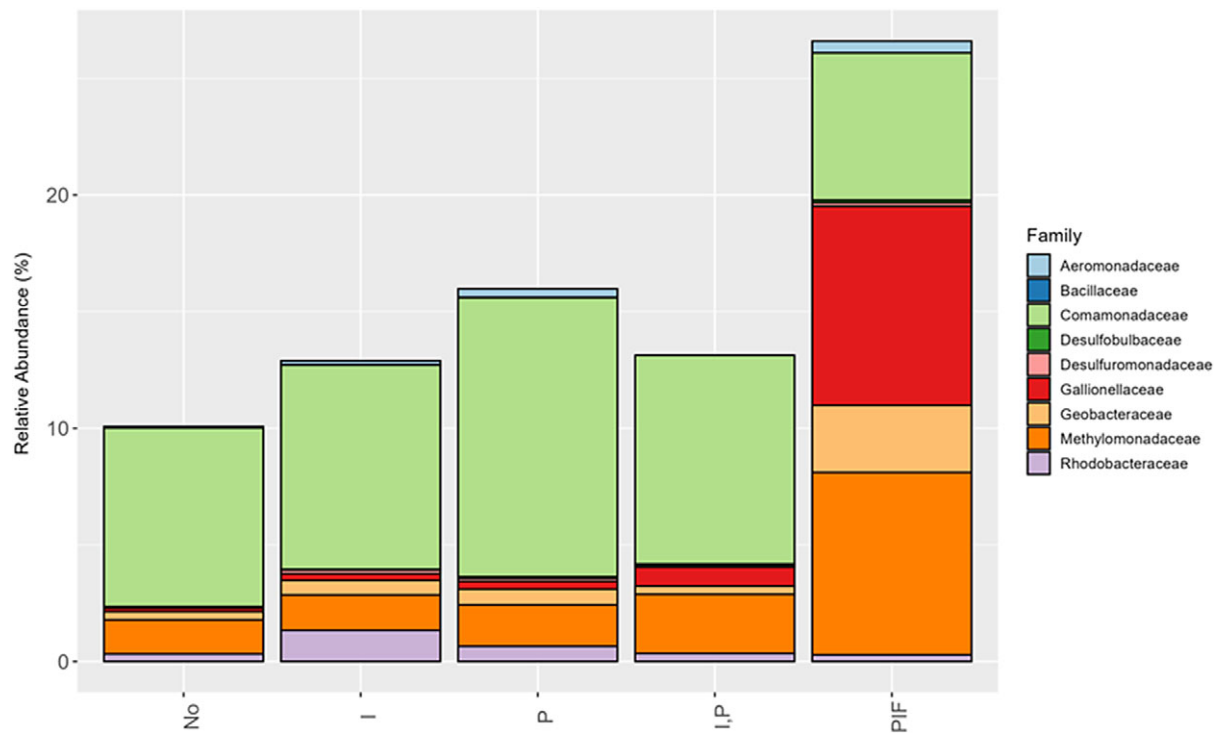
The dominant bacterial phyla detected were Bacteroidota, Proteobacteria and Actinobacteriota, respectively (Supplemental Figure 5). The pools with iridescent films and flocculent iron had higher abundances of Proteobacteria (45–70%) than the non-visible iron and solely iridescent film samples (Supplemental Figure 5).



**Figure 6.** Principal Coordinates Analyses (PCoA) conducted based on Bray-Curtis dissimilarity highlighted the distinct communities of visibly mineralised samples, which clustered on the left side of the plot, and no visible mineralisation samples, which clustered on the right side of the plot, but also included some samples that clustered with visibly mineralised samples. Ellipses are plotted with a 95% confidence interval and plotted with the percentage of variability on the axis. Variables I,P and PIF did not have enough data points to calculate the ellipse for those samples. Legend labels: No: no visible iron, I: iridescent, P: iron precipitates, I,P: both iridescence and precipitates and PIF: all three iron types. Permanova analysis revealed a  $p$ -value = 0.001.

Our results are consistent with the previous report on iron films in circumneutral wetlands, which indicated Proteobacteria were the highest abundant taxa (~80%) compared to other taxonomic groups (Dong et al., 2024). Proteobacteria's relative abundance in porewater and sediments in Mineral and Cement Creeks was between 22–78% (Hoagland et al., 2024). Moreover, previous reports support that Proteobacteria are associated with iron cycling and contribute to different iron mineralisation (Melton et al., 2014; Kappler et al., 2021), and could be important in various elemental cycling in Clear Creek. Samples clustered on the left in the PCoA (Figure 6) had a higher abundance of Proteobacteria than sample clusters on the right (Supplemental Figures 6 and 7). These findings indicate that visibly mineralised samples may encompass distinct habitats and communities compared to the non-mineralised samples.

To further investigate this, we assessed the relative abundance of 16S rRNA sequences typically assigned as iron-cycling bacteria in the different visible iron types compared to non-visible iron samples (Figure 7). Putative FeOB included the families *Gallionellaceae*, *Comamonadaceae* and *Bacillaceae*, and known FeRB included the families *Geobacteraceae*, *Aeromonadaceae*, *Desulfovibrionaceae* and *Shewanellaceae*, and *Rhodobacteraceae*, respectively (Figure 7). Not all organisms within these families are putative FeOB. We also included a family of methane oxidisers (*Methylomonadaceae*) because of their potential role in iron film formation (Dong et al., 2024). Moreover, in anoxic waters, these methane oxidisers have a syntrophic relationship with FeRB (Cabrol et al., 2020). Known iron-cycling bacteria do not make up the majority of the microbial community. Specifically, the relative abundance of FeRB found in freshwater lake sediments contained between 3 and 7%, with the highest contributions from *Geobacter* and *Desulfuromonas*, respectively (Fan et al., 2018). One study found in acid rock drainage that the relative abundance of



**Figure 7.** Relative abundance at the Family level of putative iron cycling bacteria + methane-oxidizing bacteria in the different iron mineralisation types. Legend labels: No: no visible iron, I: iridescent, P: iron precipitates, I,P: both iridescence and precipitates and PIF: all three iron types.

*Gallionella* was (1.5–4.8%) in sediments from Mineral Creek (Hoagland *et al.*, 2024), compared to our results from water samples, found *Gallionellaceae* to be between 0.5–9% in visible iron types. Within the iron films Dong *et al.* (2024) studied, *Geobacter* composed 6.8% and *Gallionella* 6.9% of the microbial community. Our visible iron types are consistent with the previous studies, with the relative abundance of iron-cycling organisms increasing by 3–17% overall compared to non-visible iron samples (Figure 7).

*Gallionellaceae* or *Comamonadaceae* were the two most abundant putative FeOB in all samples. *Comamonadaceae* has the highest abundance in mineralised samples but is similarly abundant to *Gallionellaceae* when flocculent mats are present (Figure 7). Previous studies found mineralised iron with a high abundance in both gene copies and relative abundance of *Gallionellaceae* and *Comamonadaceae* in multiple freshwater systems (Blöthe and Roden, 2009; Dong *et al.*, 2024; Fabisch *et al.*, 2013), and these bacteria have been associated with the prevalence of flocculent iron in these different aquatic systems (Brooks and Field, 2020; Williams *et al.*, 2016). The *Methylomonadaceae* relative abundance was elevated in PIF samples compared to all other samples (Figure 7).

Seasonality also affected community composition, with summer having the highest relative abundance of *Comamonadaceae* and *Methylomonadaceae*, while *Gallionellaceae* had its highest abundance in the winter (Supplemental Figure 8). Previous work in Belgium on streams to the Demer River reflected that biological oxidation could outpace the abiotic iron oxidation in the winter months, leading to increased FeOB bacteria (Baken *et al.*, 2015). Another study found similar results with *Gallionella* sp. growth observed under fully oxic conditions and neutral pH, and speculated that biological iron oxidation could outpace chemical iron oxidation at moderate or low temperatures ~13°C (de Vet *et al.*,

2011). Four areas of Graubünden canton in the Swiss Alps with 8–12°C temperatures and a pH <7.4 supported microbial iron oxidation (St Clair *et al.*, 2019). The differences in community composition in non-mineralised samples were also strongly affected by seasonality (Supplementary Figure 4).

Increased abundance of *Geobacteraceae* and *Rhodobacteraceae* in mineralised samples compared to non-mineralised supports the potential for FeRB growth following the development of hypoxic conditions in Clear Creek (Kappler *et al.*, 2021). These organisms reduce mineralised Fe(III) coupled to organic matter mineralisation, which provides energy to support the bioremediation of contaminants (Tobler *et al.*, 2007; Wu *et al.*, 2010). Studies have noted ferrihydrite or schwertmannite can drive microbial Fe(III) reduction (Sánchez-España *et al.*, 2023). Such poorly crystalline Fe(III) (oxyhydr)oxides formed from biotic iron oxidation are good substrates for FeRB coupled to organic matter oxidation. However, despite efforts to quantify poorly crystalline Fe(III) (oxyhydr)oxides in sediment iron extractions, we consistently obtained results below detection limits. The presence of FeOB and FeRB within these mineralised pools could indicate rapid microbial iron oxidation and reduction at the interface of the iron precipitates, flocculent mats and under iron films. The increased abundance of *Geobacteraceae* with *Gallionellaceae* and *Comamonadaceae* indicates the potential for this dynamic. The sites with the most damming effects contained higher abundances of iron cycling bacteria (LJ and BD) (Supplemental Figure 9), indicating the potential importance of stagnation, lowered DO and in-creek organic debris to fuel this process. Moreover, phosphorus adsorbed onto Fe(III) (oxyhydr)oxides can be released during Fe(III) reduction, which could additionally promote microbial growth within the pools (Neidhardt *et al.*, 2018).

Although the microbial community associated with iridescent films was not directly sequenced, the results from I and PIF sample types can be informative of taxa that may be associated with iron film mineralisation. Previous work has detected the families *Geobacteraceae*, *Rhodocyclusaceae*, *Gallionellaceae* and *Methylomonadaceae* (Dong et al., 2024). The presence of similar clades within our pools with films may support the idea that both FeOB and FeRB are involved in film formation. The enhanced presence of *Rhodobacteraceae* in iridescent films in our study indicates this organism may also be important to consider for a role in this process in follow-up studies.

### Iridescent iron film characterisation by SEM and TEM

While many other studies describe flocculent iron mineralisation, mineralogy and microbial processes, fewer studies describe the iridescent iron films' occurrence, characteristics and possible formation pathways (Almaraz et al., 2017; Dong et al., 2024; Grathoff et al., 2007; Sánchez-España et al., 2023). Based on our collective anecdotal experience, we suspect iridescent films may be a common mineralisation type in Clear Creek that is typically not recognised as such because of its similar appearance to organic/oil contamination. Therefore, we followed up with additional analysis to demonstrate that the iridescent film was (1) composed of iron, (2) determined the iron oxidation state and (3) ascertained the mineralogy.

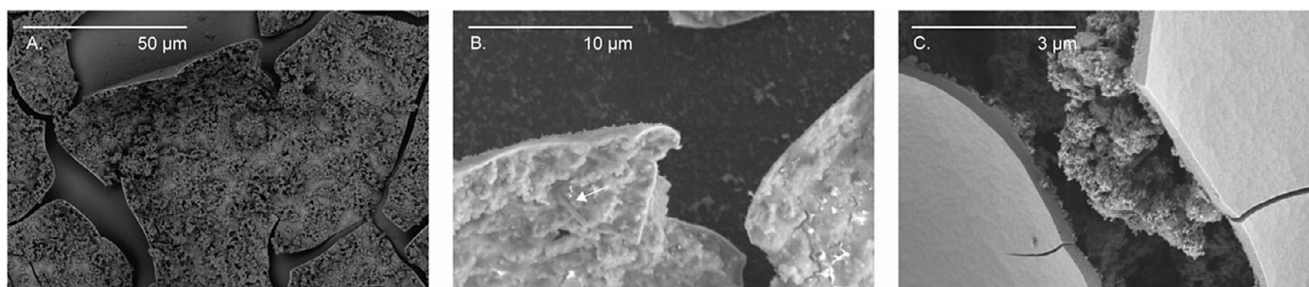
All films displayed similar characteristics when observed under both SEM and TEM. Natural film samples display cracking under SEM (Figures 8a-c), probably due to disturbance and drying during collection. Furthermore, visible rods on the films in SEM images are consistent with colonisation by bacteria (Figure 8b). At 20,000× magnification, the films appear smooth on one side and have a rough surface on the other (Figure 8c), though it was not determined which side was in contact with air vs. water in the creek. The films had a maximum thickness of 150 nm, determined in TEM (Figures 9a-b). The iridescent films were similar in chemical composition to previous work (Dong et al., 2024), containing ~70–85 at.% oxygen and ~15–30 at.% Fe as analysed by EELS (Figures 9c-d). Most films comprised these two elements; additional elements were carbon and calcium. Carbon was also present as a coating on the copper grid, making quantitative analysis of carbon exclusively from the sample impossible. A composition of 70 at.% oxygen and 30 at.% iron is consistent with Fe in 6-fold coordination with oxygen.

The oxidation state of iron in the iridescent films was assessed with EELS using the reference minerals ferrihydrite for Fe(III) and hercynite for Fe(II). The main energy loss peak based on five different analyses of the iridescent film samples is at 710 eV

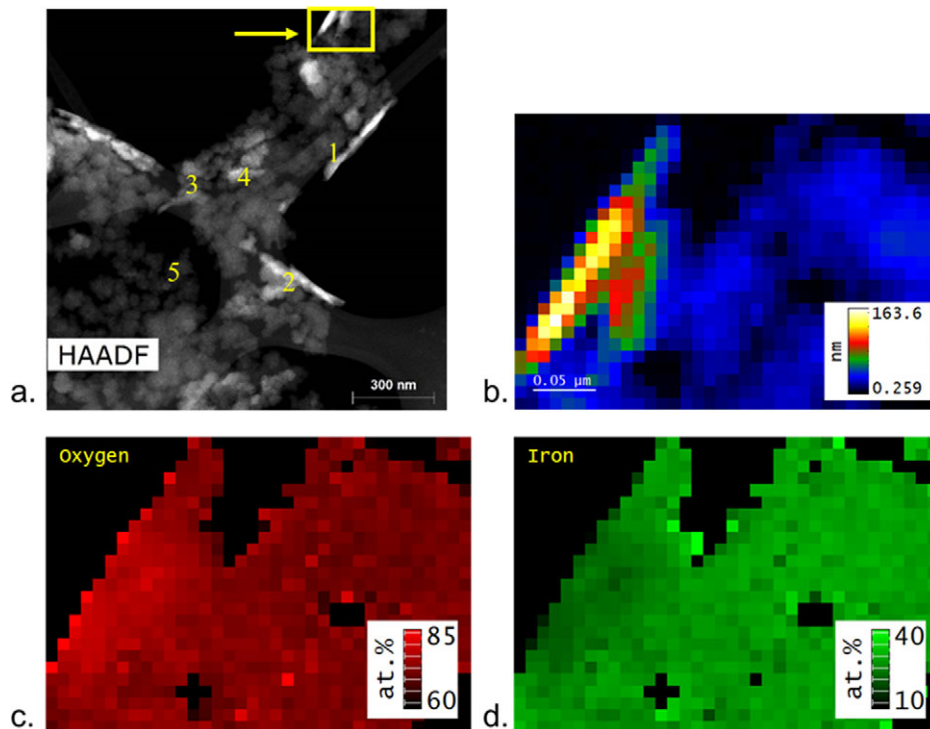
(Figures 10a-b and Supplemental Figure 10), the same energy as our ferrihydrite standard. Multiple analyses of our hercynite standard indicate it contains both Fe(II) and Fe(III) (Figure 10a). Prior studies of films found mixed valent iron or Fe(III). In the studies of Dong et al. (2024) and Grathoff et al. (2007), TEM grids were allowed to air dry, which could oxidise Fe(II). Our grids were carefully protected from oxygen until analysis, and indicate that Fe(III) can indeed be an *in situ* component of these films.

The SADP gave more mineralogical insights into the films. Two samples analysed had similar diffraction patterns with interplanar spacings at 2.11, 1.24 and 1.04 Å (Figure 11). None of these interplanar spacings corresponds to expected spacings for standard ferrihydrite and fougérite, a carbonate-bearing, mixed-valent green rust (Figure 11). An interplanar distance of  $1.226 \pm 0.031$  nm has previously been reported for a carbonate green rust (Zegeye et al., 2012). Green rust is unstable in oxygen and forms in more reducing conditions (Feder et al., 2018), where a hypoxic zone under the film could create an ideal environment for green rust formation. However, the availability of anions and parent materials such as phyllosilicates can impact the formation and crystallinity structure (Betts et al., 2023; Trolard and Bourrié 2006). The spacings in the film are offset from 2-line ferrihydrite interplanar spacings at 2.56 and 1.48 Å, although a broad ring was visible at 1.06 to 1.14 Å (Janney et al., 2000). By contrast, Grathoff et al. (2007) XRD of films showed broad peaks at 4.5, 2.6 and 1.5 Å, indicative of 2-line ferrihydrite, and was further studied by Perkins et al. (2016), finding interplanar spacings at 2.6, 3.3–3.5 and 4.4 Å that corresponded to more crystalline forms. These findings are similar to previous TEM analyses done on iridescent films from cascade pools in Northwestern Oregon, USA and the Kongjiang reservoir, where EELS was used to characterise films composed of ferrihydrite or green rust phases with Fe(II) supplied from groundwater or during microbial iron reduction (Dong et al., 2024; Perkins et al., 2016).

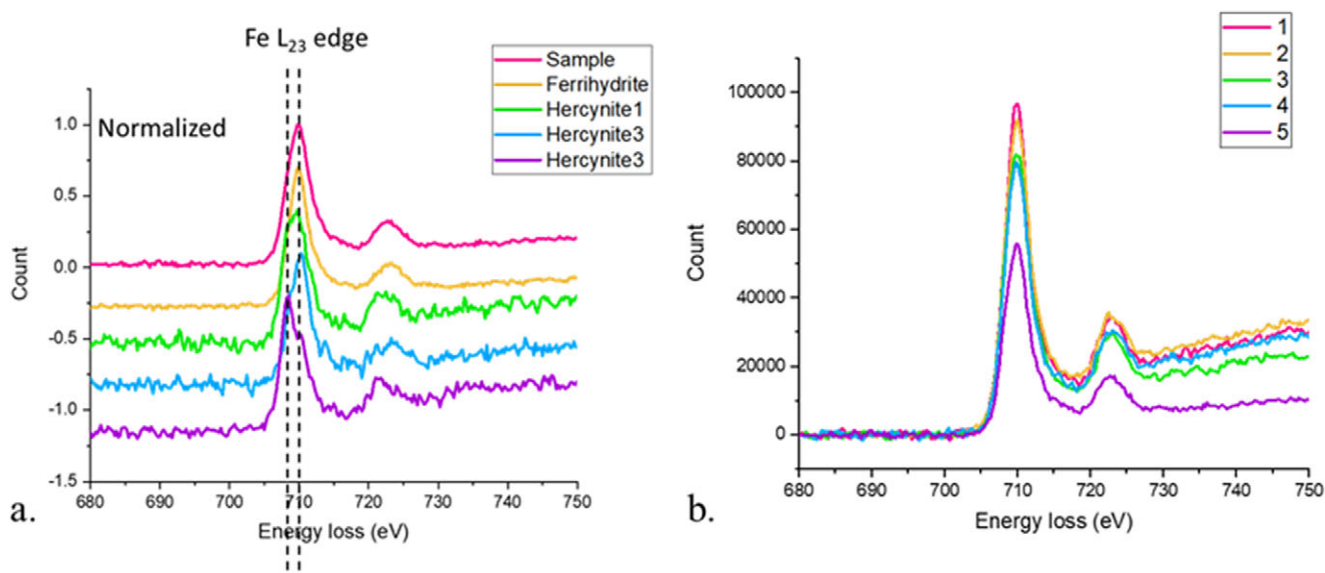
The finding that our film samples' interplanar spacings are consistent with one or more rings from 2-line ferrihydrite and carbonate-bearing green rust and lack larger spacings could be consistent with short-range order and mineral growth truncation and could be due to differences in the degree of edge-sharing within the lattice (Kleja et al., 2012; Schwertmann and Cornell, 1991; Toner et al., 2009). Disruption of crystal growth could potentially be due to the presence of dissolved ions. Environmental factors such as pH and ionic strength can influence the crystallinity of iron oxides. Specifically, silicate, carbonate and phosphate ions and organic matter can disrupt the growth of ferrihydrite crystals, leading to variations in observed ring spacings (Rutherford, 2005; Schwertmann and Cornell, 1991). Elevated OP and TP concentrations within Clear Creek compared to groundwater could disrupt



**Figures 8a-c.** SEM images of iridescent surface films ('schwimweisen') from Table 1a-c. Magnification increases through the sequence a-b-c. Minerals and/or biomass are attached to the film. The white arrow indicates a microbial rod attached to the film.



**Figures 9a-d.** TEM images of iridescent surface films ('schwimweisen') from Table 1: (a) HAADF image showing yellow inset analysed in b-d and the five areas of interest analysed by EELS in Figure 10; (b) EELS analysis to determine the thickness of the film; (c-d) percent composition of oxygen and iron.

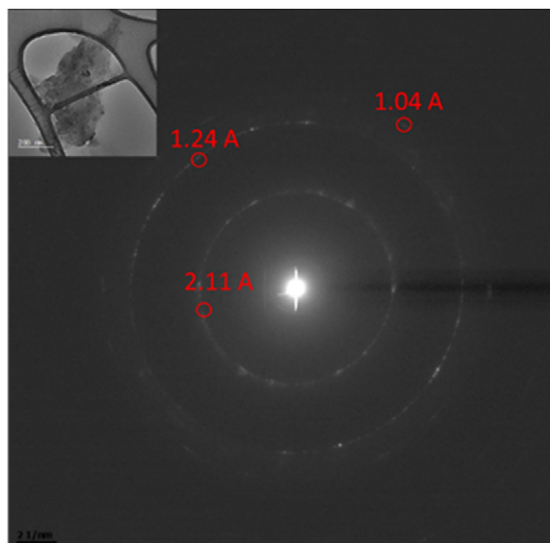


**Figures 10a-b.** EELS spectra from the iron film in Figure 6a. Reference samples (Ferrihydrate and Hercynite) were used to determine the oxidation state from Sample 1 in Figure 9b Fe L<sub>2,3</sub> edge. The legend corresponds to the 5 areas of interest labelled in Figure 9a.

mineral growth (Figure 5). The distinct lattice spacings we observed could also represent the transformation of ferrihydrite to green rust or vice versa or the disruption of crystal growth by (bi)carbonate ions. Previous work found that ferric minerals can interact with dissolved Fe(II) in anoxic environments and generate green rust (Usman *et al.*, 2012). However, these minerals are less stable, which indicates why some samples appear closer to magnetite with higher stability (Cornell and Schwertmann, 2003). Moreover, in deep-sea hydrothermal vents, it has been hypothesised that biofilms associated with Fe lack the standard crystallinity structure seen in ferrihydrite and goethite due to the

presence of Fe-complexing ligands produced biologically (Toner *et al.*, 2009).

In previous studies, organic material was observed to be attached to the films and make up a portion of the overall film composition (Kleja *et al.*, 2012; Perkins *et al.*, 2016; Dong *et al.*, 2024). An intriguing characteristic of iron films is that they float despite being mineralised of typically Fe(III) (oxyhydr)oxides that have a specific gravity of (3.3–4.3 g cm<sup>-3</sup>). The rough surface seen in (Figure 8d) could indicate the presence of co-precipitated organic matter. Perkins *et al.* (2016), indicated that humic acids were crucial for natural nanocrystalline film formation, which could create a



**Figure 11.** Representative SADP crystallography with interplanar spacings of the iridescent sample.

hydrophobic lipoprotein structure. Sánchez-España et al. (2023) noted that iron films float due to neustonic microorganisms releasing these organic compounds and exudates and acting as nucleation sites for Fe(III) mineralisation. One study found the coprecipitation of organic matter affects the mineralogy during iron cycling (Shimizu et al., 2013). Our results of short-range ordering and lack of a defined mineral structure further emphasised the need to investigate the mechanism of film formation and the co-occurring microbial and organic geochemistry. A likely scenario is that Fe(II) introduced into pools can be (re-)oxidised at the pool surface by biotic and abiotic processes (Colombo et al., 2014), possibly with ligand-based stabilisation of Fe(II). The film could form a barrier from the oxygenated surface, creating a mini-anoxic environment underneath a diverse microbial consortium of FeOB and FeRB, such as those observed from pools with films by 16S rRNA sequencing (Figure 7). Moreover, the film can form a barrier to protect the neustonic bacteria from UV or high oxygen to help promote iron and nutrient cycling as discussed by Sanchez-España et al. (2023).

## Conclusion

In this study, we report on several types of iron mineralisation in an intermittent agricultural stream in Ames, IA, USA. Sediment iron extractions and in-pool iron quantification indicate that the source of iron is not from creek water or creek sediments. Observations that mineralisation occurred in pools with elevated specific conductance relative to upstream waters and that mineralisation formed in the days following precipitation led us to hypothesise that Fe(II) was added to the creek bed by shallow groundwater discharge. Piezometers placed adjacent to the creek documented that the floodplain sediment contained mobilisable iron, the groundwater had low oxygen conditions necessary for Fe mobilisation, and a hydraulic gradient existed to drive groundwater discharge into the creek. We further postulate that in-creek organic debris that created small dams and pools, which enhanced hydraulic residence times of creek water recharged through surrounding soils and sediments, which could pick up Fe(II) from floodplain sediments.

The microbial community of pools contained putative FeOB *Gallionellaceae* and *Comomonadaceae* and putative FeRB *Geobacteraceae* and *Rhodobacteraceae*. The abundance of *Gallionellaceae* was elevated in winter, suggesting low temperatures and associated slower kinetics favour biotic over abiotic Fe(II) oxidation. The composition of FeOB and FeRB in pools with iron films was similar to what has been detected in other studies and indicates taxa to investigate their role in film formation through Fe redox cycling.

Clear Creek had iridescent films floating on the surface of pools that were characterised as short-ranged ordered minerals composed of Fe and O. Their poor crystallinity could be due to the presence of phosphate or (bi)carbonate ions that disrupted mineral growth. These floating films could represent microcosms for iron-cycling microorganisms to thrive by providing essential nutrients (*i.e.* phosphate, Fe, C, N) or a stable environment with consistent pH or DO.

We believe iron cycling is relevant to agricultural streams due to the reactivity of iron with other microbial processes and the interconnection with phosphorous cycling. Our study provides insight into a potential iron flux to a creek and highlights the importance of coupled physical and biogeochemical processes that result in the observed mineralisation. This insight into iron fluxes could be significant for other agricultural streams with intermittent iron and phosphorous inputs from groundwater or runoff, offering a broader understanding of nutrient dynamics in such ecosystems.

**Supplementary material.** The supplementary material for this article can be found at <http://doi.org/10.1180/gbi.2025.1>.

**Acknowledgements.** Thank you to Bienvenido Cortez and Faith Rahem-Seggerman for help with the R analysis. Thank you to Dr Katy Rico, Michelle Chamberlain and Dr Pete Moore for helping review the manuscript before submission. Thank you to Michelle Chamberlain, Dr Pete Moore, Luis Sosa, John Herring and Mariela Alfaro-Garcia for helping with piezometer installations. Thank you to Dr Chris Harding for help utilizing ArcGIS for Clear Creek mapping. Dr Lisa Mayhew provided the hercynite reference. Thank you to Drs Jinsu Oh, Lin Zhou and Matthew Lynn for help on the electron microscopy and related work performed using instruments in the Sensitive Instrument Facility in Ames National Lab. The Ames National Laboratory is operated for the U.S. Department of Energy by Iowa State University under Contract No. DE-AC02-07CH11358. Also, thank you to Oskar Niesen for helping collect the geochemical data.

**Funding.** This work was funded by the NSF CAREER Award: Quantifying the Extent and Biogeochemical Impact of Modern Ferruginous Lakes (Award 1944946).

## References

- Ahn J.S., Ji S.W., Cho Y.C., Youm S.J. and Yim G.J. (2015) Assessment of the potential occurrence of acid rock drainage through a geochemical stream sediment survey. *Environmental Earth Sciences*, **73**(7), 3375–3386. <https://doi.org/10.1007/s12665-014-3625-7>
- Almaraz N., Whitaker A.H., Andrews M.Y. and Duckworth O.W. (2017) Assessing Biomineral Formation by Iron-oxidizing Bacteria in a Circumneutral Creek. *Journal of Contemporary Water Research and Education*, **160**(1), 60–71. <https://doi.org/10.1111/j.1936-704x.2017.03240.x>
- Baken S., Salaets P., Desmet N., Seuntjens P., Vanlierde E. and Smolders E. (2015) Oxidation of iron causes removal of phosphorus and arsenic from streamwater in groundwater-fed lowland catchments. *Environmental Science and Technology*, **49**(5), 2886–2894. <https://doi.org/10.1021/es505834y>
- Betts A.R., Siebecker M.G., Elzinga E.J., Luxton T.P., Scheckel K.G. and Sparks D.L. (2023) Influence of clay mineral weathering on green rust formation at

- iron-reducing conditions. *Geochimica et Cosmochimica Acta*, **350** (May 2022), 46–56. <https://doi.org/10.1016/j.gca.2023.04.001>
- Blöthe M. and Roden, E.E. (2009) Microbial iron redox cycling in a circumneutral-pH groundwater seep. *Applied and Environmental Microbiology*, **75**(2), 468–473. <https://doi.org/10.1128/AEM.01817-08>
- Boano F., Harvey J.W., Marion A., Packman A.I., Revelli R., Ridolfi L. and Worman A. (2014) Hyporheic flow and transport processes: Mechanisms, models, and biogeochemical implications. *Eos, Transactions American Geophysical Union*, **69**(37), 603–679. <https://doi.org/10.1029/88EO01108>
- Boulton A.J., Findlay S., Marmonier P., Stanley E.H. and Maurice Valett H. (1998) The functional significance of the hyporheic zone in streams and rivers. *Annual Review of Ecology and Systematics*, **29**, 59–81. <https://doi.org/10.1146/annurev.ecolsys.29.1.59>
- Briggs M.A., Wang C., Day-Lewis F.D., Williams K.H., Dong W. and Lane J.W. (2019) Return flows from beaver ponds enhance floodplain-to-river metals exchange in alluvial mountain catchments. *Science of the Total Environment*, **685**, 357–369. <https://doi.org/10.1016/j.scitotenv.2019.05.371>
- Brooks C.N. and Field E.K. (2020) Iron flocs and the three domains: Microbial interactions in freshwater iron mats. *MBio*, **11**(6), 1–16. <https://doi.org/10.1128/mBio.02720-20>
- Bruun A.M., Finster K., Gunnlaugsson H.P., Nørnberg P. and Friedrich M.W. (2010) A comprehensive investigation on iron cycling in a freshwater seep including microscopy, cultivation and molecular community analysis. *Geomicrobiology Journal*, **27**(1), 15–34. <https://doi.org/10.1080/01490450903232165>
- Cabrol L., Thalasso F., Gandois L., Sepulveda-Jauregui A., Martinez-Cruz K., Teisserenc R., Tananaev N., Tveit A., Svenning M.M. and Barret M. (2020) Anaerobic oxidation of methane and associated microbiome in anoxic water of Northwestern Siberian lakes. *Science of the Total Environment*, **736**, 139588. <https://doi.org/10.1016/j.scitotenv.2020.139588>
- Callahan B.J., McMurdie P.J., Rosen M.J., Han A.W., Johnson A.J.A. and Holmes S.P. (2016) DADA2: High-resolution sample inference from Illumina amplicon data. *Nature Methods*, **13**(7), 581–583. <https://doi.org/10.1038/nmeth.3869>
- Chan C.S., Emerson D. and Luther G.W. (2016) The role of microaerophilic Fe-oxidizing micro-organisms in producing banded iron formations. *Geobiology*, **14**(5), 509–528. <https://doi.org/10.1111/gbi.12192>
- Colombo C., Palumbo G., He J.Z., Pinton R. and Cesco S. (2014) Review on iron availability in soil: Interaction of Fe minerals, plants, and microbes. In *Journal of Soils and Sediments*, **14**(3), 538–548. <https://doi.org/10.1007/s11368-013-0814-z>
- Cornell R.M. and Schwertmann U. (2003) *The iron oxides: Structure, properties, reactions, occurrences and uses*. John Wiley & Sons, UK.
- Davis N.M., Proctor Di M., Holmes S.P., Relman D.A. and Callahan B.J. (2018) Simple statistical identification and removal of contaminant sequences in marker-gene and metagenomics data. *Microbiome*, **6**(1), 1–14. <https://doi.org/10.1186/s40168-018-0605-2>
- de Vet W.W.J.M., Dinkla I. J. T., Rietveld L.C. and van Loosdrecht M.C.M. (2011) Biological iron oxidation by *Gallionella* spp. in drinking water production under fully aerated conditions. *Water Research*, **45**(17), 5389–5398. <https://doi.org/10.1016/j.watres.2011.07.028>
- Dold B., Gonzalez-Toril E., Aguilera A., Lopez-Pamo E., Cisternas M.E., Bucchi F. and Amils R. (2013) Acid Rock Drainage and Rock Weathering in Antarctica: Important Sources for Iron Cycling in the Southern Ocean. *Environmental Science and Technology*, **47**(12), 6129–6136. <https://doi.org/10.1021/es305141b>
- Dong L., Chen M., Liu C., Lv Y., Wang X., Lei Q. and Tong H. (2024) Microbe interactions drive the formation of floating iron films in circumneutral wetlands. *Science of the Total Environment*, **906** (October 2023), 167711. <https://doi.org/10.1016/j.scitotenv.2023.167711>
- Dubinsky E.A., Silver W.L. and Firestone M.K. (2010) Tropical forest soil microbial communities couple iron and carbon biogeochemistry. *Ecology*, **91**(9), 2604–2612. <https://doi.org/10.1890/09-1365.1>
- Duckworth O.W., Holmström S.J.M., Peña J. and Sposito G. (2009) Biogeochemistry of iron oxidation in a circumneutral freshwater habitat. *Chemical Geology*, **260**(3–4), 149–158. <https://doi.org/10.1016/j.chemgeo.2008.08.027>
- Emerson D. (2012) Biogeochemistry and microbiology of microaerobic Fe(II) oxidation. *Biochemical Society Transactions*, **40**(6), 1211–1216. <https://doi.org/10.1042/BST20120154>
- Emerson D., Fleming E.J. and McBeth J.M. (2010) Iron-Oxidizing Bacteria: An Environmental and Genomic Perspective. *Annual Review of Microbiology*, **64**(1), 561–583. <https://doi.org/10.1146/annurev.micro.112408.134208>
- Emerson D. and Revsbech N.P. (1994) Investigation of an iron-oxidizing microbial mat community located near Aarhus, Denmark: Field studies. *Applied and Environmental Microbiology*, **60**(11), 4022–4031. <https://doi.org/10.1128/aem.60.11.4022-4031.1994>
- Fabisch M., Beulig F., Akob D.M. and Küsel K. (2013) Surprising abundance of *Gallionella*-related iron oxidizers in creek sediments at pH 4.4 or at high heavy metal concentrations. *Frontiers in Microbiology*, **4** (Dec), 1–12. <https://doi.org/10.3389/fmicb.2013.00390>
- Fan Y.Y., Li B.B., Yang Z.C., Cheng Y.Y., Liu D.F. and Yu H.Q. (2018) Abundance and diversity of iron reducing bacteria communities in the sediments of a heavily polluted freshwater lake. *Applied Microbiology and Biotechnology*, **102**(24), 10791–10801. <https://doi.org/10.1007/s00253-018-9443-1>
- Feder F., Trolard F., Bourrié G. and Klingelhöfer G. (2018) Quantitative estimation of ferugite green rust in soils and sediments by citrate–bicarbonate kinetic extractions. *Soil Systems*, **2**(4), 1–13. <https://doi.org/10.3390/soilsystems2040054>
- Folks H.C. and Riecken F.F. (1956) Physical and Chemical Properties of Some Iowa Soil Profiles with Clay-Iron Bands. *Soil Science Society of America Journal*, **20**, 575–580. <https://doi.org/10.2136/sssaj1956.03615995002000040030x>
- Fox G.A., Purvis R.A. and Penn C.J. (2016) Streambanks: A net source of sediment and phosphorus to streams and rivers. *Journal of Environmental Management*, **181**, 602–614. <https://doi.org/10.1016/j.jenvman.2016.06.071>
- Gentry L.E., David M.B., Royer T.V., Mitchell C.A. and Starks K.M. (2007) Phosphorus Transport Pathways to Streams in Tile-Drained Agricultural Watersheds. *Journal of Environmental Quality*, **36**(2), 408–415. <https://doi.org/10.2134/jeq2006.0098>
- Grathoff G.H., Baham J.E., Easterly H.R., Gassman P. and Hugo R.C. (2007) Mixed-valent Fe films (‘schwimweisen’) on the surface of reduced ephemeral pools. *Clays and Clay Minerals*, **55**(6), 635–643. <https://doi.org/10.1346/CCMN.2007.0550610>
- Hoagland B., Navarre-Sitchler A., Cowie R. and Singha K. (2020) Groundwater–Stream Connectivity Mediates Metal(loid) Geochemistry in the Hyporheic Zone of Streams Impacted by Historic Mining and Acid Rock Drainage. *Frontiers in Water*, **2** (December), 1–25. <https://doi.org/10.3389/frwa.2020.600409>
- Hoagland B., Rasmussen K.L., Singha K., Spear J.R. and Navarre-Sitchler A. (2024) Metal-oxide precipitation influences microbiome structure in hyporheic zones receiving acid rock drainage. *Applied and Environmental Microbiology*, **90**(3). <https://doi.org/10.1128/aem.01987-23>
- Janney D.E., Cowley J.M. and Buseck P.R. (2000) Transmission electron microscopy of synthetic 2- and 6-line ferrihydrite. *Clays and Clay Minerals*, **48**(1), 111–119. <https://doi.org/10.1346/CCMN.2000.0480114>
- Kappler A., Bryce C., Mansor M., Lueder U., Byrne J.M. and Swanner E.D. (2021) An evolving view on biogeochemical cycling of iron. *Nature Reviews Microbiology*, **19**(6), 360–374. <https://doi.org/10.1038/s41579-020-00502-7>
- Kleja D.B., van Schaik J.W.J., Persson I. and Gustafsson J.P. (2012) Characterization of iron in floating surface films of some natural waters using EXAFS. *Chemical Geology*, **326–327**, 19–26. <https://doi.org/10.1016/j.chemgeo.2012.06.012>
- Kozich J.J., Westcott S.L., Baxter N.T., Highlander S.K. and Schloss P.D. (2013) Development of a dual-index sequencing strategy and curation pipeline for analyzing amplicon sequence data on the Misoq Illumina sequencing platform. *Applied and Environmental Microbiology*, **79**(17), 5112–5120. <https://doi.org/10.1128/AEM.01043-13>
- Kozubal M., Macur R.E., Korf S., Taylor W.P., Ackerman G.G., Nagy A. and Inskeep W.P. (2008) Isolation and distribution of a novel iron-oxidizing crenarchaeon from acidic geothermal springs in Yellowstone National Park. *Applied and Environmental Microbiology*, **74**(4), 942–949. <https://doi.org/10.1128/AEM.01200-07>
- Kreiling R.M., Bartsch L.A., Perner P.M., Hlavacek E.J. and Christensen V.G. (2021) Riparian Forest Cover Modulates Phosphorus Storage and Nitrogen

- Cycling in Agricultural Stream Sediments. *Environmental Management*, **68**(2), 279–293. <https://doi.org/10.1007/s00267-021-01484-9>
- Lambrecht N., Katsev S., Wittkop C., Hall S.J., Sheik C.S., Picard A. and Swanner E.D. (2020) Biogeochemical and physical controls on methane fluxes from two ferruginous meromictic lakes. *Geobiology*, **18**(1), 54–69. <https://doi.org/10.1111/gbi.12365>
- Lautz L.K. and Fanelli R.M. (2008) Seasonal biogeochemical hotspots in the streambed around restoration structures. *Biogeochemistry*, **91**(1), 85–104. <https://doi.org/10.1007/s10533-008-9235-2>
- Lautz L.K., Siegel D.I. and Bauer R.L. (2006) Impact of debris dams on hyporheic interaction along a semi-arid stream. *Hydrological Processes*, **20**(1), 183–196. <https://doi.org/10.1002/hyp.5910>
- Lawrence J.E., Skold M.E., Hussain F.A., Silverman D.R., Resh V.H., Sedlak D.L., Luthy R.G., and McCray J.E. (2013) Hyporheic zone in urban streams: A review and opportunities for enhancing water quality and improving aquatic habitat by active management. *Environmental Engineering Science*, **30**(8), 480–501. <https://doi.org/10.1089/ees.2012.0235>
- Lefler F.W., Berthold D.E. and Laughinghouse H.D. (2023) Cyanoseq: A database of cyanobacterial 16S rRNA gene sequences with curated taxonomy. *Journal of Phycology*, **59**(3), 470–480. <https://doi.org/10.1111/jpy.13335>
- Lovley D.R. (1987) Organic matter mineralisation with the reduction of ferric iron: A review. *Geomicrobiology Journal*, **5**(3–4), 375–399. <https://doi.org/10.1080/01490458709385975>
- McMurdie, P.J., and Holmes, S. (2013) phyloseq: An R Package for Reproducible Interactive Analysis and Graphics of Microbiome Census Data. *PLOS ONE*, **8**(4), e61217. <https://doi.org/10.1371/journal.pone.0061217>
- Melton E.D., Swanner E.D., Behrens S., Schmidt C. and Kappler A. (2014) The interplay of microbially mediated and abiotic reactions in the biogeochemical Fe cycle. *Nature Reviews Microbiology*, **12**(12), 797–808. <https://doi.org/10.1038/nrmicro3347>
- Méndez-García C., Peláez A.I., Mesa V., Sánchez J., Golyshina O.V. and Ferrer M. (2015) Microbial diversity and metabolic networks in acid mine drainage habitats. *Frontiers in Microbiology*, **6** (MAY), 1–17. <https://doi.org/10.3389/fmicb.2015.00475>
- Mori J.F., Neu T.R., Lu S., Händel M., Totsche K.U. and Küsel K. (2015) Iron encrustations on filamentous algae colonized by Gallionella-related bacteria in a metal-polluted freshwater stream. *Biogeosciences*, **12**(18), 5277–5289. <https://doi.org/10.5194/bg-12-5277-2015>
- Murphy J. and Riley J.P. (1962) A modified single solution method for the determination of phosphate in natural waters. *Analytica Chimica Acta*, **27**(C), 31–36. [https://doi.org/10.1016/S0003-2670\(00\)88444-5](https://doi.org/10.1016/S0003-2670(00)88444-5)
- Neidhardt H., Schoeckle D., Schleinitz A., Eiche E., Berner Z., Tram P.T.K., Lan V.M., Viet P.H., Biswas A., Majumder S., Chatterjee D., Oelmann Y. and Berg M. (2018) Biogeochemical phosphorus cycling in groundwater ecosystems – Insights from South and Southeast Asian floodplain and delta aquifers. *Science of the Total Environment*, **644**, 1357–1370. <https://doi.org/10.1016/j.scitotenv.2018.07.056>
- Perkins R.B., Gray Z.N., Grathoff G. and Hugo R. (2016) Characterization of natural and synthetic floating iron surface films and their associated waters. *Chemical Geology*, **444**, 16–26. <https://doi.org/10.1016/j.chemgeo.2016.09.027>
- Pierson B.K. and Parenteau M.N. (2000) Phototrophs in high iron microbial mats: Microstructure of mats in iron-depositing hot springs. *FEMS Microbiology Ecology*, **32**(3), 181–196. [https://doi.org/10.1016/S0168-6496\(00\)00018-0](https://doi.org/10.1016/S0168-6496(00)00018-0)
- Rentz J.A., Kraiya C., Luther G.W. and Emerson D. (2007) Control of ferrous iron oxidation within circumneutral microbial iron mats by cellular activity and autocatalysis. *Environmental Science and Technology*, **41**(17), 6084–6089. <https://doi.org/10.1021/es062203e>
- Rentz J.A., Turner I.P. and Ullman J.L. (2009) Removal of phosphorus from solution using biogenic iron oxides. *Water Research*, **43**(7), 2029–2035. <https://doi.org/10.1016/j.watres.2009.02.021>
- Rivett M.O., Ellis P.A. and Mackay R. (2011) Urban groundwater baseflow influence upon inorganic river-water quality: The River Tame headwaters catchment in the City of Birmingham, UK. *Journal of Hydrology*, **400**(1–2), 206–222. <https://doi.org/10.1016/j.jhydrol.2011.01.036>
- Roden E.E., McBeth J.M., Blöthe M., Percak-Dennett E.M., Fleming E.J., Holyoke R.R., Luther G.W., Emerson D. and Schieber J. (2012) The microbial ferrous wheel in a neutral pH groundwater seep. *Frontiers in Microbiology*, **3** (May), 1–18. <https://doi.org/10.3389/fmicb.2012.00172>
- Rosenberg B.D. and Schroth A.W. (2017) Coupling of reactive riverine phosphorus and iron species during hot transport moments: Impacts of land cover and seasonality. *Biogeochemistry*, **132**(1–2), 103–122. <https://doi.org/10.1007/s10533-016-0290-9>
- Rowden R.D. (2010) *The Iowa State-Wide Trace Element Soil Sampling Project: Design and Implementation*. (June), 1–78. Iowa Department of Natural Resources, Iowa City, USA.
- Rutherford J.S. (2005) Crystal Structure. Pp. 289–294 in: *Encyclopedia of Condensed Matter Physics* (F. Bassani, G.L. Liedl and P.B.T.-E. Wyder, editors). <https://doi.org/10.1016/B0-12-369401-9/00686-0>
- Sánchez-España J., Ilin A.M., Yusta I., van der Graaf C.M. and Sánchez-Andrea I. (2023) Fe(III) Biomineralisation in the Surface Microlayer of Acid Mine Waters Catalyzed by Neustonic Fe(II)-Oxidizing Microorganisms. *Minerals*, **13**(4). <https://doi.org/10.3390/min13040508>
- Sarkkola S., Nieminen M., Koivusalo H., Laurén A., Kortelainen P., Mattsson T., Palviainen M., Piirainen S., Starr M. and Finér L. (2013) Iron concentrations are increasing in surface waters from forested headwater catchments in eastern Finland. *Science of The Total Environment*, 463–464, 683–689. <https://doi.org/10.1016/j.scitotenv.2013.06.072>
- Schilling K.E., Kim S., Jones C.S. and Wolter C.F. (2017) Orthophosphorus Contributions to Total Phosphorus Concentrations and Loads in Iowa Agricultural Watersheds. *Journal of Environmental Quality*, **46**(4), 828–835. <https://doi.org/10.2134/jeq2017.01.0015>
- Schwertmann U. and Cornell R.M. (1991) *Iron Oxides in the Laboratory: Preparation and Characterization*. VCH, Weinheim, Germany.
- Shimizu M., Zhou J., Schröder C., Obst M., Kappler A. and Borch T. (2013) Dissimilatory reduction and transformation of ferrihydrite-humic acid coprecipitates. *Environmental Science and Technology*, **47**(23), 13375–13384. <https://doi.org/10.1021/es402812j>
- Sobolev D. and Roden E.E. (2002) Evidence for rapid microscale bacterial redox cycling of iron in circumneutral environments. *Antonie van Leeuwenhoek, International Journal of General and Molecular Microbiology*, **81**(1–4), 587–597. <https://doi.org/10.1023/A:1020569908536>
- Soto-Varela F., Rodríguez-Blanco M.L., Taboada-Castro M.M. and Taboada-Castro M.T. (2015) Metals discharged during different flow conditions from a mixed agricultural-forest catchment (NW Spain). *Hydrological Processes*, **29**(6), 1644–1655. <https://doi.org/10.1002/hyp.10282>
- St Clair B., Pottenger J., Debes R., Hanselmann K. and Shock E. (2019) Distinguishing Biotic and Abiotic Iron Oxidation at Low Temperatures. *ACS Earth and Space Chemistry*, **3**(6), 905–921. <https://doi.org/10.1021/acsearthspacechem.9b00016>
- Stookey L.L. (1970) Ferrozine-A New Spectrophotometric Reagent for Iron. *Analytical Chemistry*, **42**(7), 779–781. <https://doi.org/10.1021/ac60289a016>
- Tobler N.B., Hofstetter T.B., Straub K.L., Fontana D. and Schwarzenbach R.P. (2007) Iron-mediated microbial oxidation and abiotic reduction of organic contaminants under anoxic conditions. *Environmental Science and Technology*, **41**(22), 7765–7772. <https://doi.org/10.1021/es071128k>
- Toner B.M., Santelli C.M., Marcus M.A., Wirth R., Chan C.S., McCollom T., Bach W. and Edwards, K.J. (2009) Biogenic iron oxyhydroxide formation at mid-ocean ridge hydrothermal vents: Juan de Fuca Ridge. *Geochimica et Cosmochimica Acta*, **73**(2), 388–403. <https://doi.org/10.1016/j.gca.2008.09.035>
- Trolard F. and Bourrié G. (2006) Structure of fougérite and green rusts and a thermodynamic model for their stabilities. *Journal of Geochemical Exploration*, **88**(1-3 Spec. Iss.), 249–251. <https://doi.org/10.1016/j.gexplo.2005.08.048>
- USGS (2022) *StreamStats Report*, 1–13. United States Geological Survey, Boulder, Colorado, USA.
- Usman M., Hanna K., Abdelmoula M., Zegeye A., Faure P. and Ruby C. (2012) Formation of green rust via mineralogical transformation of ferric oxides (ferrihydrite, goethite and hematite). *Applied Clay Science*, **64**, 38–43. <https://doi.org/10.1016/j.clay.2011.10.008>
- Viollier E., Inglett P.W., Hunter K., Roychoudhury A.N. and Van Cappellen P. (2000) The ferrozine method revisited: Fe(II)/Fe(III) determination in natural waters. *Applied Geochemistry*, **15**, 785–790. doi: 10.1016/S0883-2927(99)00097-9
- Williams M.R., Wessel B.M. and Filoso S. (2016) Sources of iron (Fe) and factors regulating the development of flocculate from Fe-oxidizing bacteria in regenerative streamwater conveyance structures. *Ecological Engineering*, **95**, 723–737. <https://doi.org/10.1016/j.ecoleng.2016.06.120>

- Wu C.Y., Zhuang L., Zhou S.G., Li F.B. and Li X.M. (2010) Fe(III)-enhanced anaerobic transformation of 2,4-dichlorophenoxyacetic acid by an iron-reducing bacterium *Comamonas koreensis* CY01. *FEMS Microbiology Ecology*, **71**(1), 106–113. <https://doi.org/10.1111/j.1574-6941.2009.00796.x>
- Yang C., Zhang Y.K., Liu Y., Yang X. and Liu C. (2018) Model-Based Analysis of the Effects of Dam-Induced River Water and Groundwater Interactions on Hydro-Biogeochemical Transformation of Redox Sensitive Contaminants in a Hyporheic Zone. *Water Resources Research*, **54**(9), 5973–5985. <https://doi.org/10.1029/2018WR023286>
- Zegeye A., Bonneville S., Benning L.G., Sturm A., Fowle D.A., Jones C.A., Canfield D.E., Ruby C., MacLean L.C., Nomosatryo S., Crowe S.A. and Poulton S.W. (2012) Green rust formation controls nutrient availability in a ferruginous water column. *Geology*, **40**(7), 599–602. <https://doi.org/10.1130/G32959.1>
- Zhang X., Müller M., Jiang S., Wu Y., Zhu X., Mujahid A., Zhu Z., Fakharuddin Muhamad M., Sien Aun Sia E., Holt Ajon Jang F. and Zhang J. (2020) Distribution and flux of dissolved iron in the peatland-draining rivers and estuaries of Sarawak, Malaysian Borneo. *Biogeosciences*, **17**(7), 1805–1819. <https://doi.org/10.5194/bg-17-1805-2020>